K-Ras^{V14I} recapitulates Noonan syndrome in mice

Isabel Hernández-Porras[a], Salvatore Fabbiano[b], Alberto J. Schuhmacher[a,1], Alexandra Aicher[c], Marta Cañamero[d,2], Juan Antonio Cámara[d], Lorena Cussó[e,f,g], Manuel Desco[e,f,g], Christopher Heeschen[c], Francisca Mulero[d], Xosé R. Bustelo[b], Carmen Guerra[a,3], and Mariano Barbacid[a,3]

[a]Molecular Oncology, [c]Molecular Pathology, and [d]Biotechnology Programs, Centro Nacional de Investigaciones Oncológicas, E-28029 Madrid, Spain; [b]Centro de Investigación del Cáncer, Universidad de Salamanca, E-37007 Salamanca, Spain; [e]Departamento de Bioingeniería e Ingeniería Aeroespacial, Universidad Carlos III, E-28911 Madrid, Spain; [f]Instituto de Investigación Sanitaria Gregorio Marañón, E-28007 Madrid, Spain; and [g]Centro de Investigación Biomédica en Red de Salud Mental, E-28029 Madrid, Spain

Contributed by Mariano Barbacid, October 3, 2014 (sent for review May 16, 2014; reviewed by Allan Balmain, Bronwyn Kerr, and Martin Zenker)

Noonan syndrome (NS) is an autosomal dominant genetic disorder characterized by short stature, craniofacial dysmorphism, and congenital heart defects. NS also is associated with a risk for developing myeloproliferative disorders (MPD), including juvenile myelomonocytic leukemia (JMML). Mutations responsible for NS occur in at least 11 different loci including *KRAS*. Here we describe a mouse model for NS induced by K-*Ras*^{V14I}, a recurrent *KRAS* mutation in NS patients. K-*Ras*^{V14I}–mutant mice displayed multiple NS-associated developmental defects such as growth delay, craniofacial dysmorphia, cardiac defects, and hematologic abnormalities including a severe form of MPD that resembles human JMML. Homozygous animals had perinatal lethality whose penetrance varied with genetic background. Exposure of pregnant mothers to a MEK inhibitor rescued perinatal lethality and prevented craniofacial dysmorphia and cardiac defects. However, Mek inhibition was not sufficient to correct these defects when mice were treated after weaning. Interestingly, Mek inhibition did not correct the neoplastic MPD characteristic of these mutant mice, regardless of the timing at which the mice were treated, thus suggesting that MPD is driven by additional signaling pathways. These genetically engineered K-*Ras*^{V14I}–mutant mice offer an experimental tool for studying the molecular mechanisms underlying the clinical manifestations of NS. Perhaps more importantly, they should be useful as a preclinical model to test new therapies aimed at preventing or ameliorating those deficits associated with this syndrome.

RASopathies | developmental disorders | heart defects | myeloproliferative disorders | MEK inhibitors

Noonan syndrome (NS) (1) belongs to a group of clinically related developmental disorders known as "RASopathies" (2, 3). NS presents with an incidence of about 1/1,000–1/2,500 newborns, and patients display a broad spectrum of clinical symptoms including craniofacial dysmorphia, short stature, cardiovascular and skeletal defects, delayed puberty, and learning difficulties (4). About 10% of NS patients also exhibit myeloproliferative disorders (MPD), which usually are transient. Less frequently, these patients develop severe MPD, juvenile myelomonocytic leukemia (JMML), or other forms of leukemia (2, 5). NS is inherited in an autosomal dominant manner and results from germ-line mutations in at least 11 different genes including Protein Tyrosine Phosphatase Non-Receptor type 11 (*PTPN11*), Son of Sevenless homolog 1 (*SOS1*), *KRAS*, *NRAS*, *RAF1*, *BRAF*, *MEK1*, *SHOC2*, *CBL*, *RIT1*, and *RRAS*, most of which are involved in mediating RAS signaling (3, 6–8). Among these loci, *PTPN11* is the most frequently mutated, in about 50% of NS patients. *KRAS* mutations have been identified in less than 5% of the patients (2).

NS patients with *KRAS* mutations display more severe clinical and cognitive defects. However, the limited number of these patients makes it difficult to establish a clear genotype–phenotype correlation (3, 4). Thus, far, 18 different germ-line mutations have been reported in the *KRAS* locus of NS patients (NSEuroNet database: nseuronet.com). These mutations confer milder gain-of-function effects than somatically acquired cancer-associated mutations (9). Replacement of the valine residue located at position 14 by isoleucine is one of the most frequent *KRAS* mutations (10). Although this mutation is adjacent to amino acid residues typically altered in cancer, KRAS^{V14I} displays an intermediate intrinsic GTPase activity compared with wild-type and oncogenic isoforms (9). Moreover, the mutant KRAS^{V14I} protein shows an increase in nucleotide exchange activity that is likely to be responsible for its accumulation in the active guanosine triphosphate (GTP)-bound state (9).

Here we describe the generation of a strain of mice carrying an endogenous K-*Ras*^{V14I} germ-line mutation. These mice displayed many of the phenotypic abnormalities observed in NS patients, including small size, craniofacial dysmorphism, and cardiac defects. Moreover, they develop fatal MPD, a disease reminiscent of the JMML characteristic of patients with NS. These mice offer a relevant experimental tool for studying the alterations underlying the clinical manifestations of NS and for testing new therapies aimed at preventing or ameliorating these deficits.

Results

Generation of K-*Ras*^{V14I}–Mutant Mice. To generate a K-*Ras*^{V14I} mouse model for NS, we introduced a GTA (Val) to ATA (Ile) mutation in codon 14 of the endogenous K-*Ras* locus by homologous recombination (Fig. S1). K-*Ras*$^{+/V14I}$–mutant mice were born at the expected Mendelian ratios, reached adulthood,

Significance

Noonan syndrome (NS) is a developmental disorder caused by germ-line mutations in various components of the RAS signaling pathway. The pathophysiological mechanisms underlying the clinical manifestations in NS patients and the basis for the observed phenotypic variability are poorly understood. To date, mouse models carrying mutations in Protein Tyrosine Phosphatase Non-Receptor type 11 (*Ptpn11*), Son of Sevenless homolog 1 (*Sos1*), and *Raf1* loci have been described. The new model described here, induced by K-*Ras*^{V14I} expression, recapitulates most of the NS features including small size, craniofacial dysmorphism, cardiac defects, and myeloproliferative disorders, highly reminiscent of juvenile myelomonocytic leukemia. These mice should help us understand better the phenotypic variations of NS and serve as a preclinical tool to test forthcoming therapies based on the design of novel inhibitors of the RAS pathway.

Author contributions: C.G. and M.B. designed research; I.H.-P., S.F., A.J.S., A.A., J.A.C., and L.C. performed research; A.A., M.C., J.A.C., L.C., M.D., C.H., F.M., and X.R.B. analyzed data; and I.H.-P., C.G., and M.B. wrote the paper.

Reviewers: A.B., University of California, San Francisco Helen Diller Family Comprehensive Cancer Center; B.K., Central Manchester University Hospitals NHS Foundation Trust; and M.Z., University Hospital Magdeburg.

The authors declare no conflict of interest.

[1]Present address: Cancer Cell Biology Programme, Spanish National Cancer Research Center, E-28029 Madrid, Spain.

[2]Present address: Roche Pharmaceutical Research and Early Development, Translational Medicine Oncology, Roche Innovation Center Penzberg, 82377 Penzberg, Germany.

[3]To whom correspondence may be addressed. Email: mcguerra@cnio.es or mbarbacid@cnio.es.

This article contains supporting information online at www.pnas.org/lookup/suppl/doi:10.1073/pnas.1418126111/-/DCSupplemental.

and were fertile (Table S1). In contrast, homozygous K-*Ras*$^{V14I/V14I}$ animals (hereafter referred to as "K-*Ras*^{V14I} mice") had significant perinatal lethality, probably because of heart insufficiency and hematopoietic defects (see below). These mutant mice were backcrossed to the 129S2/Sv (hereafter referred to as "129 mice") or C57BL/6J (hereafter referred to as "B6 mice") background for several generations. Heterozygous mice were viable for at least seven generations in both genetic backgrounds. However, homozygous K-*Ras*^{V14I} mice backcrossed for five generations resulted in either increased (in 129 mice) or complete (in B6 mice) perinatal lethality (Table S1). These observations indicate the existence of modifier alleles that modulate the phenotypic consequences of K-*Ras*^{V14I} expression. All the studies described in this article were carried out with mice of a mixed B6/129 background, unless otherwise indicated.

Molecular Analysis of K-Ras Signaling Pathways. To determine the degree of activation of the mutant K-Ras^{V14I} protein, we obtained cell extracts from wild-type and mutant embryos at embryonic day 13.5 (E13.5) and incubated them with the Ras-binding domain (RBD) of the c-Raf kinase (Fig. S2*A*). As expected, the amount of K-Ras protein bound to RBD was more abundant in K-*Ras*$^{+/V14I}$ and K-*Ras*^{V14I} than in wild-type embryos. However, the amount of K-Ras^{V14I} bound to RBD was lower than that observed in mouse embryonic fibroblasts (MEFs) expressing the oncogenic K-Ras^{G12V} isoform (Fig. S2*A*). These observations support the concept that the level of activation of the K-Ras^{V14I} protein is somewhat intermediate between the wild-type and the oncogenic K-Ras isoforms (9). Despite the increased levels of active RBD-bound K-Ras^{V14I} proteins in K-*Ras*$^{+/V14I}$ and K-*Ras*^{V14I} embryos, their primary signaling pathways were not overly activated. As illustrated in Fig. S2*B*, the phosphorylation levels of the Mek, Erk, and Akt downstream kinases were similar in wild-type and mutant E13.5 embryos. Likewise, we could not detect significant differences in adult tissues such as spleen and heart, two of the organs most affected by the expression of the K-Ras^{V14I} isoform (see below) (Fig. S2*B*). These observations are reminiscent of those previously observed in a mouse model for Costello syndrome driven by germ-line expression of a mutant H-Ras^{G12V} isoform (11). However, immunohistochemical (IHC) analysis of the mutant hearts revealed increased levels of phosphoErk expression at all stages, including embryonic development (E13.5 and E18.5), birth (postnatal day 0, P0), and adulthood (P120) (Fig. S2 *C* and *D*). In addition, MEFs isolated from K-*Ras*^{V14I}–mutant mice displayed a higher growth rate than wild-type MEFs. As expected, their proliferation could be inhibited by MEK inhibitors (Fig. S2*E*). However, Erk phosphorylation appeared to be equally sensitive to MEK inhibitors in wild-type and mutant K-*Ras* MEFs, including those expressing K-Ras^{V14I} as well as the oncogenic K-Ras^{G12V} isoform (Fig. S2*F*). Moreover, when these cells were exposed to EGF, the activation kinetics of their Erk and Akt downstream pathways and the extent of their response were similar to those observed in wild-type MEFs (Fig. S2*G*).

Reduced Body Size and Facial Dysmorphia in K-*Ras*^{V14I} Mice. K-*Ras*$^{+/V14I}$ mice, regardless of their genetic background, were similar in weight and body size to wild-type animals. K-*Ras*^{V14I} mice also had normal size and weight at birth. However, surviving animals were significantly smaller at weaning (Fig. 1*A*). Moreover, at 4 wk of age, K-*Ras*^{V14I} males weighed only 72% [11.7 ± 2.22 g (n = 18) vs. 16.3 ± 3.97 g (n = 24)] and were 23% shorter [(7.1 ± 4.26 cm (n = 7) vs. 8.2 ± 2.27 cm (n = 6)] than their wild-type littermates (Fig. 1 *A* and *B*). These differences were ameliorated by age 3 mo, especially in mice of mixed B6/129 genetic background (Fig. 1*A*). More importantly, K-*Ras*$^{+/V14I}$ and K-*Ras*^{V14I} mice had a reduced life span, with half-lives of 62 and 36 wk, respectively (Fig. 1*C*).

K-*Ras*^{V14I} mice exhibited facial dysmorphia reminiscent of other NS mouse models (12–14) as well as of NS patients (4). They are characterized by a pronounced triangular facial appearance with a shorter distance between the ears and the nose, blunter snout, and wider separation between the eyes (Fig. 1*B*). Analysis of 4-mo-old male mice (n = 6) by micro X-ray computed tomography (micro-CT) revealed increased skull width and height along with reduced length, resulting in a rounder skull with bigger volume (Fig. 1*D* and Table S2). Consistent with a gene-dose effect, these alterations were less pronounced in heterozygous mice (Table S2).

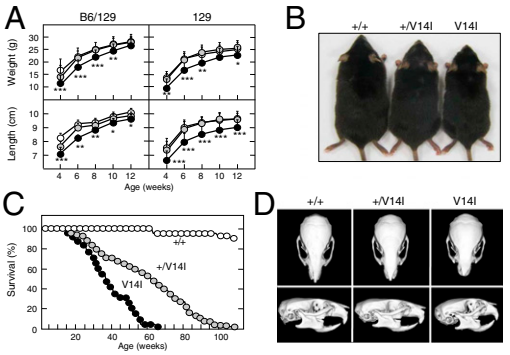

Fig. 1. NS-like developmental defects in K-*Ras*^{V14I} mice. (*A*) Growth curves of male mice in mixed B6/129 and 129 (F5) genetic backgrounds. (*Upper*) Body weight of wild-type (n = 24 and 14, respectively) (open circles), K-*Ras*$^{+/V14I}$ (n = 36 and 22, respectively) (gray circles), and K-*Ras*^{V14I} (n = 18 and 8, respectively) (solid circles) male mice. (*Lower*) Body length of wild-type (n = 6 and 14, respectively) (open circles), K-*Ras*$^{+/V14I}$ (n = 14 and 22, respectively) (gray circles), and K-*Ras*^{V14I} (n = 7 and 8, respectively) (solid circles) male mice. Error bars indicate SD. *P < 0.05; **P < 0.01; ***P < 0.001. (*B*) Representative image of 4-mo-old wild-type (+/+), K-*Ras*$^{+/V14I}$ (+/V14I), and K-*Ras*^{V14I} (V14I) male mice. (*C*) Survival curve of wild-type (n = 25) (+/+, open circles), K-*Ras*$^{+/V14I}$ (n = 68) (+/V14I, gray circles), and K-*Ras*^{V14I} (n = 30) (V14I, solid circles) mice in mixed B6/129 genetic background. (*D*) Representative micro-CT scans of skulls from 4-mo-old wild-type (+/+), K-*Ras*$^{+/V14I}$ (+/V14I), and K-*Ras*^{V14I} (V14I) male mice in mixed B6/129 genetic background. See Table S2 for morphometric measurements.

K-*Ras*^{V14I} Mice Developed Heart Abnormalities. K-*Ras*^{V14I} mice displayed cardiac hyperplasia. This defect already was evident in E13.5 embryos (Fig. S3*A*). Careful histological analysis of K-*Ras*^{V14I} mice that died at P0 (n = 5) revealed focal necrosis in tissues such as liver and muscle, consistent with defects associated with a cardiovascular etiology (Fig. S3*B*). At 4 mo of age, cardiac hyperplasia was characterized by a significant increase in heart/body weight ratio (Fig. 2*A*). Histological analysis revealed a substantial thickening of all chambers (Fig. 2*B*). We did not observe tissue fibrosis or other gross alterations in the histological structure of auricles or ventricles. However, aortic valves were thicker in mutant mice (Fig. 2*B*). The increased size of K-*Ras*^{V14I} hearts was caused by increased numbers of cardiomyocytes, not by increased cell size (Fig. 2*C*). Ki67 staining revealed a higher proliferation rate in cardiomyocytes of 4-mo-old K-*Ras*^{V14I} mice than in wild-type controls (Fig. 2*D*). Heterozygous animals displayed similar, albeit less pronounced, phenotypes (Fig. 2).

We next investigated whether cardiac stem cells might contribute to the cardiac phenotype of K-*Ras*^{V14I} animals. We observed an expansion of the Sca-1^{+}/PDGFRα^{+}/CD31^{-} cardiac stem cells from hearts of unweaned (P10–P14) mice (Fig. S3*C*). Moreover, when we cultured sorted cardiac stem cells, we observed increased numbers of colonies in the cultures containing cells isolated from the mutant K-*Ras*$^{+/V14I}$ mice as compared with cultures of cells derived from their wild-type littermates (Fig. S3*D*). We also studied the expression of genes associated with pluripotency in the hearts of these unweaned animals. We observed a 14-fold increase in the expression of *Nanog* and a threefold down-regulation of *miR-100*, an miRNA known to be repressed in undifferentiated embryonic stem cells (Fig. S3 *E* and *F*) (15). As expected, targets of *miR-100*,

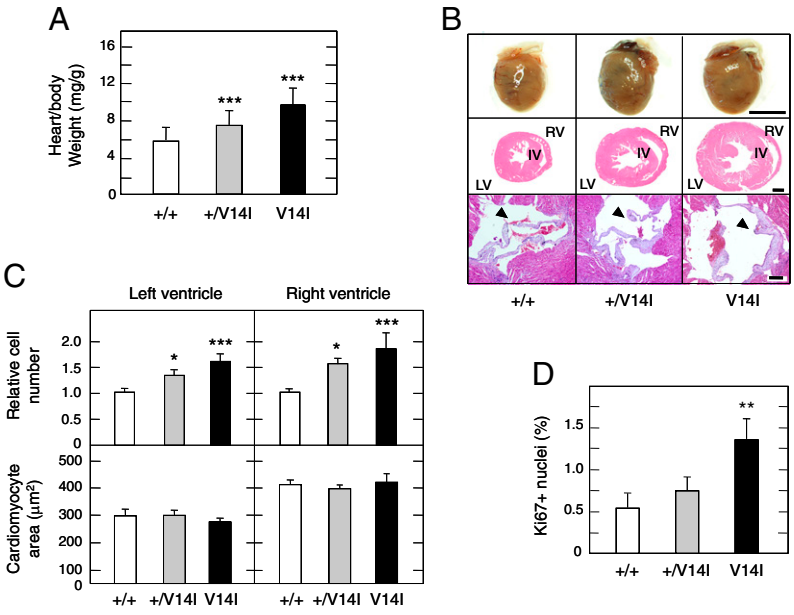

Fig. 2. Heart defects in 4-mo-old K-*Ras*^{V14I} male mice. (*A*) Heart/body weight ratio of wild-type (n = 22) (+/+, open bars), K-*Ras*$^{+/V14I}$ (n = 30) (+/V14I, gray bars), and K-*Ras*^{V14I} (n = 13) (V14I, solid bars) mice. (*B*) Histology of the heart. (*Top*) Formalin-fixed hearts. (Scale bar: 0.5 cm.) (*Middle*) H&E-stained heart ventricular sections. Interventricular wall (IV), right ventricle (RV), and left ventricle (LV) are indicated. (Scale bar: 1 mm.) (*Bottom*) H&E-stained aortic valves. Solid arrowheads point to aortic valves. (Scale bar: 50 μm.) (*C*) Cardiomyocyte hyperplasia. Relative cardiomyocyte number (*Upper*) and cardiomyocyte area (*Lower*) per ventricle of 4-mo-old wild-type (n = 8) (+/+, open bars), K-*Ras*$^{+/V14I}$ (n = 12) (+/V14I, gray bars), and K-*Ras*^{V14I} (n = 3) (V14I, solid bars) mice. (*D*) Percentage of Ki67-positive cardiomyocytes in wild-type (n = 5) (+/+, open bars), K-*Ras*$^{+/V14I}$ (n = 5) (+/V14I, gray bars), and K-*Ras*^{V14I} (n = 5) (V14I, solid bars) mice. Error bars indicate SD. *P < 0.05; **P < 0.01; ***P < 0.001.

such as *Mkk6* and *Smarca5*, were found to be up-regulated in the mutant cells (Fig. S3*F*).

To analyze cardiac morphology and function, we performed MRI studies on 4-mo-old mice. As expected, wall thickness in systole, systolic wall thickening, and left ventricle mass were increased significantly in K-*Ras*^{V14I} mice as compared with their wild-type littermates. Accordingly, K-*Ras*^{V14I} hearts showed increased end diastolic volume. End systolic volume remained normal, indicating preserved or enhanced function. Consistent with this interpretation, fractional shortening and cardiac output were increased in K-*Ras*^{V14I} mice. No differences were found in the wall thickness in diastole, ejection fraction, or heart rate (Table S3). Despite these changes, K-*Ras*^{V14I} mice did not display hypertension, heart fibrosis, or cardiovascular remodeling. No major differences where found in either renal morphology or histology, although the kidneys frequently showed infiltration from hematopoietic cells (Fig. S4*A*).

Hematologic Defects in K-*Ras*^{V14I} Mice. NS patients often have hepatosplenomegaly, and some develop MPD (2–4). At 4 mo of age, K-*Ras*^{V14I} animals (n = 12) displayed severe splenomegaly (Fig. 3*A*). Heterozygous K-*Ras*$^{+/V14I}$ mice (n = 22) also had enlarged spleens, albeit to a more limited extent (Fig. 3*A*). This anomaly was caused by congestion and increased extramedullary hematopoiesis (Fig. 3*B*). Histopathological analysis also revealed lymphoid and myeloid infiltrates in a variety of organs, including liver, kidney, and lung (Fig. S4*A*). K-*Ras*^{V14I} mice (n = 10) suffered from anemia and thrombocytopenia and showed a significant increase in the number of leukocytes in peripheral blood, mainly because of the expansion of neutrophils, eosinophils, and basophils (Fig. 3*B* and Table S4). Flow cytometry analysis revealed significant expansion of myeloid cells in the spleen of K-*Ras*^{V14I}–mutant mice (n = 14) with increased levels of both Gr1$^+$/CD11b$^+$ double-positive and CD11b$^+$ single-positive cells (Fig. 3*C* and Fig. S4*B*). The increased percentage of myeloid cells was associated with a concomitant decrease in the percentage of CD3$^+$ T cells, as the result of a significant decrease of CD8$^+$ T cells (Fig. S4*C*). However, the percentage of CD19$^+$ B cells and CD4$^+$ T cells in mutant mice was comparable to that in wild-type littermates (Fig. S4*C*). The proliferative capacity of bone marrow (BM) progenitors was assayed in methylcellulose medium in presence of IL-3 and GM-CSF. BM cells of K-*Ras*$^{+/V14I}$ and K-*Ras*^{V14I} mice, but not those of wild-type littermates, proliferated in the absence of cytokines. Moreover, they proliferated more robustly than control BM cells in the presence of cytokines (Fig. 3*D*). Taken together, these results indicate that germ-line expression of the mutant K-Ras^{V14I} protein leads to the development of hematological disorders including MPD.

To investigate the mechanism by which K-*Ras*^{V14I} mice developed MPD, we analyzed the BM of 4-mo-old K-*Ras*^{V14I} animals (n = 9) for the presence of Lin$^-$/Sca-1$^+$/c-Kit$^+$ (LSK) cells, a population known to be enriched for hematopoietic stem cells (HSCs). As illustrated in Fig. 4 *A* and *B*, K-*Ras*^{V14I} mice displayed a significant increase in LSK cells. These mutant cells had a proliferative index, based on BrdU uptake, similar to that observed in cells obtained from control littermates (Fig. S4*D*). However, the mutant LSK cells had reduced levels of annexin V, a marker for apoptotic cells (Fig. S4*E*). These results indicate that the expansion of the HSC population in K-*Ras*^{V14I} mice is caused by decreased programmed cell death rather than by enhanced cell proliferation. Multiparameter flow cytometry analysis also revealed increased numbers of committed progenitors, including a significant increase in common myeloid progenitors (CMPs) (Lin$^-$/IL7Rα$^-$/Sca-1$^-$/c-Kit$^+$/FcγR^{low}/CD34$^+$) and granulocyte-macrophage progenitors (GMPs) (Lin$^-$/IL7Rα$^-$/Sca-1$^-$/c-Kit$^+$/FcγR^{high}/CD34$^+$) and a slight increase in common lymphoid progenitors (CLPs) (Lin$^-$/IL7Rα$^+$/Sca-1^{low}/c-Kit^{low}). The number of megakaryocyte-erythroid progenitors (MEPs) (Lin$^-$/IL7Rα$^-$/Sca-1$^-$/c-Kit$^+$/FcγR^{low}/CD34$^-$) did not display significant alterations (Fig. 4*C* and Fig. S4*F*). These observations suggest that expression of the K-Ras^{V14I} oncoprotein promotes expansion of both HSCs and committed precursors of the myeloid lineage.

Stem Cell Origin of K-Ras^{V14I}–Driven MPD. To determine whether the MPD displayed by K-*Ras*^{V14I} mice was caused by the expansion of HSCs, we transplanted BM cells from K-*Ras*$^{+/+}$ (n = 20) and K-*Ras*$^{+/V14I}$ (n = 14) mice backcrossed to the B6 background for four generations into lethally irradiated B6 recipients. Peripheral blood of recipient mice was analyzed at various intervals (2–34 wk) after transplantation. These BM cells, regardless of whether they were obtained from wild-type or K-*Ras*$^{+/V14I}$ mice, efficiently reconstituted the entire hematopoietic system in the recipient mice. However, only the animals transplanted with BM cells derived from K-*Ras*$^{+/V14I}$ mice developed MPD between 30 and 34 wk after transplantation. In these mice, WBC counts in their peripheral blood were increased, mainly because of the expansion of neutrophils, eosinophils, and basophils (Table S4). Spleens of mice reconstituted with BM cells carrying

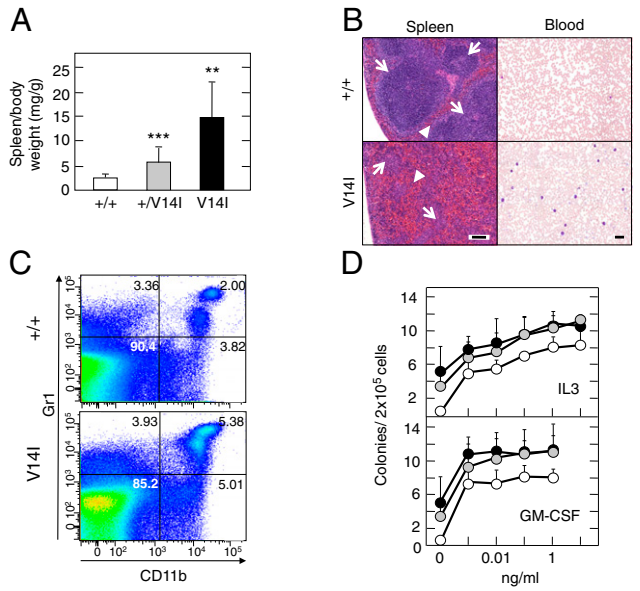

Fig. 3. Hematological disorders in K-*Ras*^{V14I} mice. (*A*) Spleen/body weight ratio in 4-mo-old wild-type (n = 13) (+/+, open bars), K-*Ras*$^{+/V14I}$ (n = 22) (+/V14I, gray bars), and K-*Ras*^{V14I} (n = 12) (V14I, solid bars) male mice. (*B*) H&E-stained paraffin-embedded sections of spleen and peripheral blood smears stained with May–Grünwald/Giemsa of 4-mo-old wild-type (+/+) and K-*Ras*^{V14I} (V14I) mice. White and red pulp are indicated by arrows and arrowheads, respectively. (Scale bars: 100 μm for spleen; 20 μm for blood smears). (*C*) Flow cytometry analysis of Gr1$^+$ and CD11b$^+$ cells in spleens of 4-mo-old wild-type (+/+) and K-*Ras*^{V14I} (V14I) mice. (*D*) Number of myeloid colonies formed by BM cells obtained from 4-mo-old wild-type (n = 3) (open circles), K-*Ras*$^{+/V14I}$ (n = 3) (gray circles), and K-*Ras*^{V14I} (n = 3) (solid circles) mice in the absence or presence of the indicated concentrations of IL-3 and GM-CSF. Error bars indicate SD. $^{**}P < 0.01$; $^{***}P < 0.001$.

the K-*Ras*^{V14I} mutation were enlarged (Fig. S4 *G* and *H*) and displayed increased levels of CD11b$^+$ and Gr1$^+$/CD11b$^+$ myeloid cells (Fig. S4*I*). Finally, the percentages of LSK cells and of CMP and GMP progenitors also were increased significantly in the BM of the reconstituted mice (Fig. S4 *J* and *K*).

Inhibition of the Mek Kinase During Embryonic and Early Postnatal Development Prevented NS Defects. We also investigated whether pharmacological inhibition of K-Ras signaling could ameliorate the defects observed in K-*Ras*^{V14I} mice. To this end, we exposed pregnant mothers (n = 8) to the MEK inhibitor PD0325901 (a daily i.p. injection 1 mg/kg of body weight) from E7.5 until P9, followed by direct treatment of the pups (i.p., every other day) until P21. Two hours after the last injection, tissues were taken to determine the effect of the MEK inhibitor on K-Ras^{V14I} signaling using phosphoErk as a readout. As illustrated in Fig. S5*A*, the MEK inhibitor efficiently inhibited Erk phosphorylation in wild-type and K-*Ras*^{V14I} animals, although in the latter the inhibition was only partial. Despite the incomplete inhibition, this treatment completely rescued perinatal lethality. Only 13% (4/31) of the K-*Ras*^{V14I} mice treated with vehicle were alive at weaning, whereas in mice exposed to the MEK inhibitor the percentage was that expected from Mendelian ratios (16/56 or 29%). Treatment with the MEK inhibitor also rescued the heart defects observed in neonatal (P0) mice (Fig. S5*B*) as well as the increase in Sca-1$^+$/PDGFRα$^+$/CD31$^-$ cardiac stem cells in unweaned K-*Ras*$^{+/V14I}$ mice (Fig. S5*C*). Furthermore, treated mice analyzed at P0 showed a reduction in phosphoErk levels in the heart as compared with the untreated mice (Fig. S5*D*). This reduction correlated with a decrease in the proliferation of cardiac cells as illustrated by Ki67 immunostaining (Fig. S5*E*).

Mek inhibition also prevented the craniofacial dysmorphia and growth defects even after the treatment was discontinued. Four-month-old K-*Ras*^{V14I} mice (n = 9) exposed to the MEK inhibitor from E7.5 to P21 retained normal skulls (Table S5) as well as hearts of normal size (Fig. 5*A* and Fig. S5*F*) and with normal numbers of cardiomyocytes (Fig. 5*B*). These observations indicate that the deleterious effects caused by abnormal K-Ras^{V14I} signaling do not affect bone development or heart homeostasis beyond weaning, the time when the animals were no longer exposed to MEK inhibitors.

Treated K-*Ras*$^{+/V14I}$ mice also survived longer into adulthood. As illustrated in Fig. 6*A*, K-*Ras*$^{+/V14I}$ mice (n = 6) treated with vehicle had a median survival of 58 wk, but those exposed to the inhibitor from E7.5 to P21 (n = 12) survived an average of 75 wk, a 30% increase. Likewise, the median survival of K-*Ras*^{V14I} mice (n = 9) treated with the MEK inhibitor was 30% longer than that of littermates (n = 6) exposed to vehicle (48 vs. 37 wk) (Fig. 6*A*). Unfortunately, all mice succumbed to MPD. Indeed, treated K-*Ras*$^{+/V14I}$ and K-*Ras*^{V14I} mice had enlarged spleens caused by the expansion of myeloid cells (Gr1$^+$ and

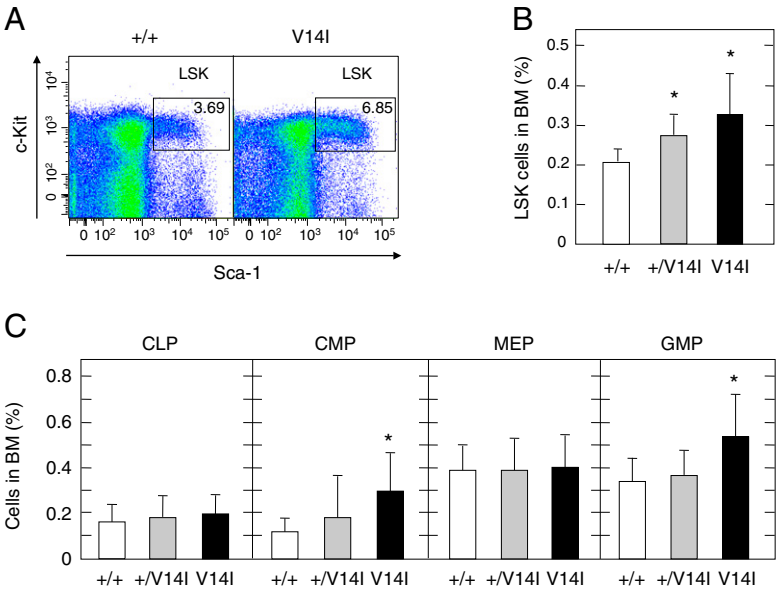

Fig. 4. Aberrant hematopoiesis in 4-mo-old K-*Ras*^{V14I} mice. (*A*) Flow cytometry analysis of freshly harvested BM cells of wild-type (+/+) and K-*Ras*^{V14I} (V14I) mice using antibodies against c-Kit and Sca-1. The percentage of LSK cells is indicated. (*B*) Percentage of LSK cells in the BM of wild-type (n = 11) (+/+, open bars), K-*Ras*$^{+/V14I}$ (n = 15) (+/V14I, gray bars), and K-*Ras*^{V14I} (n = 9) (V14I, solid bars) mice. (*C*) Frequencies of CLP, CMP, MEP, and GMP populations in BM cells were quantified in wild-type (n = 11) (+/+, open bars), K-*Ras*$^{+/V14I}$ (n = 15) (+/V14I, gray bars), and K-*Ras*^{V14I} (n = 9) (V14I, solid bars) mice. Error bars indicate SD. $^{*}P < 0.05$.

$CD11b^+/Gr1^+$) (Fig. S5 *G* and *H*). These mutant mice also had increased numbers of LSK progenitor cells in their BM (Fig. S5*I*). Thus, Mek inhibition during embryonic and early postnatal development slowed down progression but did not prevent MPD.

Inhibition of the Mek Kinase in Young and Adult K-*Ras*^{V14I} Mice. Next, we examined the effect of interfering with K-Ras^{V14I} signaling after postnatal development. A cohort of P21 K-*Ras*^{V14I} mice ($n = 12$) was treated with the PD0325901 inhibitor (5 mg/kg body weight i.p. daily) for 6 wk (up to P63). Under these experimental conditions the MEK inhibitor blocked phosphorylation of the Erk kinases to the same extent as in mice treated during embryonic development (Fig. S5*A*). However, this treatment did not prevent or even ameliorate the developmental defects characteristic of K-*Ras*^{V14I} mice, including decreased size and body weight, craniofacial dysmorphia, and cardiac defects. The survival of treated K-*Ras*$^{+/V14I}$ mice was increased by 40% to 71 wk ($n = 12$) vs. the 51-wk average survival observed in untreated littermates ($n = 11$) (Fig. 6*B*). However, these mice also underwent expansion of myeloid cells in the spleen and of LSK progenitor cells in the BM and succumbed to MPD. No increase in survival was observed in treated K-*Ras*^{V14I} mice ($n = 5$), which had a median survival of 38 wk.

Finally, we used the MEK inhibitor (5 mg/kg body weight i.p. daily for 4 wk) to treat adult (4-mo-old) K-*Ras*$^{+/V14I}$ mice ($n = 11$) that already displayed signs of MPD to determine whether inhibition of the Mek kinases might provide some therapeutic benefit. MPD was diagnosed by detection of enlarged spleens using micro-CT scans as well as by altered blood counts (leukocytosis and anemia). Unfortunately, this treatment did not reduce spleen size or increase the median survival of the treated mice (Fig. 6*C*). Taken together, these observations suggest that pathways other than the canonical Raf/Mek/Erk signaling cascade must contribute to the development of MPD in K-*Ras*^{V14I}–mutant mice.

Discussion

Mutations in *RAS* genes have been implicated in various RASopathies, mainly Costello syndrome (*HRAS*) and NS (*KRAS* and *NRAS*) (2, 3). To understand better their role in these developmental disorders and to provide an experimental platform for the development of future anti-RAS therapies, we have generated mouse models for Costello syndrome [H-*Ras*^{G12V} mice (11)] and for NS (this study). K-*Ras*$^{+/V14I}$ and K-*Ras*^{V14I} mice displayed smaller size at weaning, craniofacial dysmorphia, and cardiac and hematopoietic defects, including the development of MPD. These defects are reminiscent of human NS-like features also observed in other mouse models of NS carrying mutations in *Ptpn11*, *Sos1*, and *Raf1* (12–14).

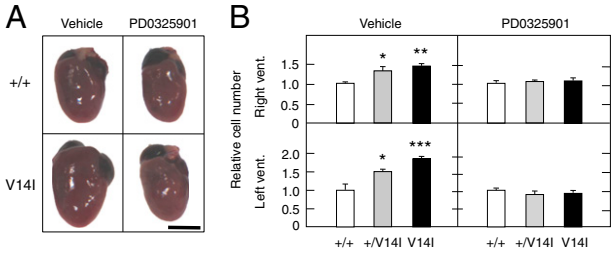

Fig. 5. Treatment of K-*Ras*^{V14I} mice with the MEK inhibitor PD0325901 during embryonic and early postnatal development prevents developmental defects. (*A*) Representative hearts of 4-mo-old wild-type (+/+) and K-*Ras*^{V14I} (V14I) male mice exposed to vehicle or PD0325901 from E7.5 to P21. (Scale bar: 5 mm.) (*B*) Relative number of cardiomyocytes in the right and left ventricles of 4-mo-old wild-type (+/+, open bars), K-*Ras*$^{+/V14I}$ (+/V14I, gray bars), and K-*Ras*^{V14I} (V14I, solid bars) male mice exposed from E7.5 to P21 to vehicle ($n = 11$, $n = 13$; $n = 6$, respectively) or to PD0325901 ($n = 4$, $n = 8$; $n = 8$, respectively). Error bars indicate SD. $^*P < 0.05$; $^{**}P < 0.01$; $^{***}P < 0.001$.

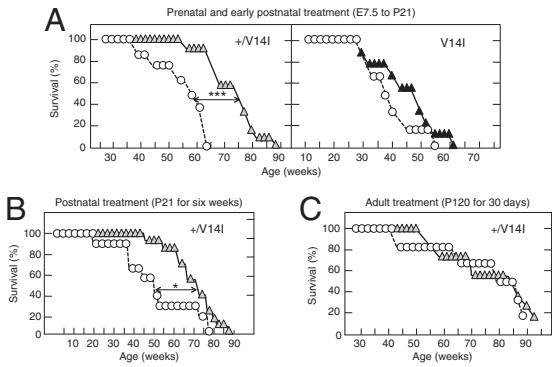

Fig. 6. Survival of K-*Ras*$^{+/V14I}$ and K-*Ras*^{V14I} mice exposed to the MEK inhibitor PD0325901 at prenatal, postnatal, and adult stages. (*A*) Survival of K-*Ras*$^{+/V14I}$ (+/V14I) and K-*Ras*^{V14I} (V14I) mice exposed from E7.5 to P21 to vehicle ($n = 8$ and $n = 6$, respectively; open circles, dashed lines) or to PD0325901 ($n = 12$ and $n = 9$, respectively; gray and solid triangles, respectively, solid lines). $^{***}P < 0.001$. (*B*) Survival of K-*Ras*$^{+/V14I}$ (+/V14I) mice exposed for 6 wk beginning at P21 (until P64) to vehicle ($n = 11$, open circles, dashed line) or to PD0325901 ($n = 12$, gray triangles, solid line). $^*P < 0.05$. (*C*) Survival of K-*Ras*$^{+/V14I}$ (+/V14I) mice exposed at 4 mo of age (P120) for 30 d to vehicle ($n = 6$, open circles, dashed line) or to PD0325901 ($n = 11$, gray triangles, solid line).

Expression of the mutant K-Ras^{V14I} protein, unlike its oncogenic isoforms, allows embryonic and postnatal development. However, the number of K-*Ras*^{V14I} mice obtained from heterozygous crosses was significantly lower than expected, indicating that the increased dosage of the mutant K-Ras^{V14I} protein affects embryonic development. As previously observed in the H-*Ras*^{G12V} strain (11), K-*Ras*$^{+/V14I}$ and K-*Ras*^{V14I} embryos and affected adult tissues do not display significant biochemical alterations in Ras signaling, suggesting the existence of negative feedback mechanisms. It also is possible that Western blot analysis of phosphorylated downstream effectors using whole-organ extracts might not be sensitive enough to identify changes in signaling output present in defined populations of cells. Indeed, IHC analysis revealed increased levels of phosphoErk in both embryonic and adult mutant hearts.

K-*Ras*^{V14I} mice display heart hyperplasia caused by an increased number of cardiomyocytes associated with increased thickening of the aortic valve. However, heart function in these mice appears to be normal, as illustrated by MRI studies. This phenotype is significantly different from those observed in NS models carrying mutations in other loci. For instance, *Ptpn11*$^{+/D61G}$ mice display septal defects with no cardiac hypertrophy (12). On the other hand, *Sos1*$^{+/E846K}$ mice developed left ventricular hypertrophy with incompletely penetrant aortic stenosis, ventricular fibrosis, epicardial fibrosis, and adipocyte infiltration (13). Finally, *Raf1*$^{+/L613V}$ mice had normal valvuloseptal development but exhibited eccentric cardiac hypertrophy that decompensated upon pressure overload (14). The severity of these heart defects appears to be responsible for the shorter life span of these strains and for the embryonic lethality of homozygous *Ptpn11*^{D61G} and *Sos1*^{E846K} mice (12, 13).

The cardiac defects observed in K-*Ras*^{V14I} animals also are different from those of H-*Ras*^{G12V} mice (11). In H-*Ras*^{G12V} mice the increase in heart size resulted from cardiomyocyte hypertrophy caused by AngII-dependent hypertension, but in the K-*Ras*^{V14I} strain it was a direct consequence of a higher number of cardiomyocytes, possibly caused by an expansion of cardiac stem cells, a phenotype also observed in a B-*Raf*–driven model that recapitulates some of the clinical features of cardio-facio-cutaneous syndrome patients (16). Whether these differences are caused by the specific effect of certain members of the Ras signaling machinery on cardiac stem and/or progenitor cells remains to be determined. Other factors, such as quantitative differences in downstream signaling or the contribution of

DEVELOPMENTAL BIOLOGY

modifier genes, also may account for the distinct nature of the heart alterations found in these mouse models.

About 25% of pediatric NS patients display some degree of hepatosplenomegaly. A more limited number develop a benign form of MPD that regresses spontaneously in most cases (17, 18). However, some NS patients occasionally develop JMML, a fatal form of MPD characterized by cytokine hypersensitivity of myeloid progenitors (18). K-*Ras*^{V14I} mice developed a fatal MPD highly reminiscent of human JMML. This MPD was similar to that observed in *Nf1*$^{+/-}$ animals and mice selectively expressing oncogenic K-*Ras*^{G12D} alleles in hematopoietic progenitors (19–21) and differed from that observed in mice carrying heterozygous mutations in the *Ptpn11*, *Sos1*, and *Raf1* loci, which had a slower onset and a less aggressive nature (12–14).

One of the main goals of developing mouse models that faithfully reproduce human pathologies is to use them as experimental tools for preclinical testing of novel drug therapies. MEK inhibitors have been approved for the treatment of *BRAF* oncogene-driven metastatic melanomas (22, 23) and currently are being tested in clinical trials for *KRAS* oncogene-driven tumors. Although these inhibitors exhibit significant toxic effects that limit their therapeutic utility in RASopathies at present, it is possible that they could be used at lower, safer doses, given the significantly lower levels of RAS activity in these developmental syndromes. Indeed, a phase II trial (NCT01556568) to assess the safety and efficacy of a MEK inhibitor in adult NS patients with hypertrophic cardiomyopathy has been initiated recently. Our results indicate that exposing the developing embryo to well-tolerated doses of the MEK inhibitor PD0325901 prevents the appearance of the main developmental defects present in K-*Ras*^{V14I} mice. These observations open the door for the potential therapeutic use of RAS inhibitors to prevent the developmental defects in children carrying NS mutations.

Unfortunately, our results indicate that exposure of young mice to a MEK inhibitor had little benefit. None of the developmental defects were prevented or cured in mice treated with the MEK inhibitor at weaning. However, the treated K-*Ras*$^{+/V14I}$ mice displayed 40% increased survival, presumably because of a deceleration in the development of MPD. Similar experiments were carried out with the same MEK inhibitor in NS models induced by *Sos1*^{E846K} and *Raf1*^{L613V} alleles (13, 14). Prenatal treatment of *Sos1*^{E846K} mice rescued embryonic lethality, reduced the penetrance of cardiac defects, and improved, but did not correct, size and craniofacial dysmorphia (13). Postnatal treatment of *Raf1*^{L613V} mice normalized cardiac and growth defects. However, facial dysmorphia was rescued only when the treatment started at P0 (14).

Clinical testing of MEK and/or other inhibitors in pregnant mothers and infant NS carriers will require careful analysis of potential toxic effects of these compounds. Moreover, MEK inhibitors do not seem to be sufficient to prevent or cure MPD. Additional inhibitors of RAS signaling might yield useful results in treating MPD in NS patients, possibly by inducing synergistic effects with MEK inhibitors. Available mouse models for NS, including the one described here, should serve as invaluable tools to test future therapeutic strategies to treat the various pathologies that characterize this developmental disorder.

Methods

Generation of K-*Ras*^{V14I} Mice. The strategy used to generate the K-*Ras*^{V14I} strain and genotyping protocols are described in *SI Methods*. Mice were housed in a barrier facility according to animal care standards established by the European Union. All the experiments were reviewed and approved by the Animal Care Committee of the Institute of Health Carlos III and the University of Salamanca.

Micro-CT and MRI. Micro-CT images were acquired according to standard protocols with an eXplore Vista PET-CT (GE Healthcare) using an amperage of 200 μA and a voltage of 35 kV (11). Skull measurements from micro-CT scans and MRI images were carried out as described in *SI Methods*.

Flow Cytometry Analysis, Colony-Formation Assay, and BM Transplantation. Single-cell suspensions were obtained from BM and spleen and were stained as described in *SI Methods*. Detailed information about the colony-formation assay and BM transplantation can be found in *SI Methods*.

Inhibitor Treatment. The MEK inhibitor PD0325901 was synthesized by Wuhan Sunrise Technology Development Company, Ltd. Its preparation and administration are described in *SI Methods*.

ACKNOWLEDGMENTS. We thank I. Agudo, I. Aragón, N. Cabrera, M. C. González, B. Jiménez, M. Lamparero, M. Ligós, P. Nogales, M. San Román, T. Teixeira, and R. Villar for technical assistance. We also acknowledge the support of the Histopathology and Transgenic Units. We thank J. Pastor and S. Martinez for providing the MEK inhibitor. Work was supported by grants from the European Research Council (ERC-AG/250297-RAS AHEAD), European Union Framework Programme (LSHG-CT-2007-037665, HEALTH-F2-2010-259770, and HEALTH-2010-260791), Spanish Ministry of Science and Innovation (SAF2006-11773 and CSD2007-00017), Spanish Ministry of Economy and Competitiveness (SAF2011-30173), Autonomous Community of Madrid (GR/SAL/0587/2004 and S2006/BIO-0232), and Fundación de la Mutua Madrileña del Automovil (to M.B.); by grants from the Spanish Ministry of Economy and Competitiveness (SAF2009-07172, SAF2012-3171, RD06/0020/0001, and RD12/0036/0002), the Castilla-León Autonomous Government (CSI039A12-1), and the Asociación Española Contra el Cáncer (AECC) (to X.R.B.); and by grants from Fondo de Investigación Sanitaria (PI042124, PI08-1623, PI11-02529), Autonomous Community of Madrid (GR/SAL/0349/2004), and Fundación Ramón Areces (FRA 01-09-001) (to C.G.). I.H.-P. was supported by a fellowship from the Instituto de Salud Carlos III, and S.F. and A.J.S. were supported by fellowships from the Spanish Ministry of Economy and Competitiveness.

1. Noonan JA, Ehmke DA (1963) Associated noncardiac malformations in children with congenital heart disease. *Midwest Soc Pediatr Res* 63:468–470.
2. Schubbert S, Shannon K, Bollag G (2007) Hyperactive Ras in developmental disorders and cancer. *Nat Rev Cancer* 7(4):295–308.
3. Rauen KA (2013) The RASopathies. *Annu Rev Genomics Hum Genet* 14:355–369.
4. Roberts AE, Allanson JE, Tartaglia M, Gelb BD (2013) Noonan syndrome. *Lancet* 381(9863):333–342.
5. Jongmans MC, et al. (2011) Cancer risk in patients with Noonan syndrome carrying a PTPN11 mutation. *Eur J Hum Genet* 19(8):870–874.
6. Aoki Y, et al. (2013) Gain-of-function mutations in RIT1 cause Noonan syndrome, a RAS/MAPK pathway syndrome. *Am J Hum Genet* 93(1):173–180.
7. Flex E, et al. (2014) Activating mutations in RRAS underlie a phenotype within the RASopathy spectrum and contribute to leukaemogenesis. *Hum Mol Genet* 23(16):4315–4327.
8. Tartaglia M, Gelb BD, Zenker M (2011) Noonan syndrome and clinically related disorders. *Best Pract Res Clin Endocrinol Metab* 25(1):161–179.
9. Gremer L, et al. (2011) Germline KRAS mutations cause aberrant biochemical and physical properties leading to developmental disorders. *Hum Mutat* 32(1):33–43.
10. Lo FS, et al. (2009) Noonan syndrome caused by germline KRAS mutation in Taiwan: Report of two patients and a review of the literature. *Eur J Pediatr* 168(8):919–923.
11. Schuhmacher AJ, et al. (2008) A mouse model for Costello syndrome reveals an Ang II-mediated hypertensive condition. *J Clin Invest* 118(6):2169–2179.
12. Araki T, et al. (2004) Mouse model of Noonan syndrome reveals cell type- and gene dosage-dependent effects of Ptpn11 mutation. *Nat Med* 10(8):849–857.
13. Chen PC, et al. (2010) Activation of multiple signaling pathways causes developmental defects in mice with a Noonan syndrome–associated Sos1 mutation. *J Clin Invest* 120(12):4353–4365.
14. Wu X, et al. (2011) MEK-ERK pathway modulation ameliorates disease phenotypes in a mouse model of Noonan syndrome associated with the Raf1(L613V) mutation. *J Clin Invest* 121(3):1009–1025.
15. Tarantino C, et al. (2010) miRNA 34a, 100, and 137 modulate differentiation of mouse embryonic stem cells. *FASEB J* 24(9):3255–3263.
16. Urosevic J, et al. (2011) Constitutive activation of B-Raf in the mouse germ line provides a model for human cardio-facio-cutaneous syndrome. *Proc Natl Acad Sci USA* 108(12):5015–5020.
17. Bader-Meunier B, et al. (1997) Occurrence of myeloproliferative disorder in patients with Noonan syndrome. *J Pediatr* 130(6):885–889.
18. Hasle H (2009) Malignant diseases in Noonan syndrome and related disorders. *Horm Res* 72(Suppl 2):8–14.
19. Jacks T, et al. (1994) Tumour predisposition in mice heterozygous for a targeted mutation in Nf1. *Nat Genet* 7(3):353–361.
20. Braun BS, et al. (2004) Somatic activation of oncogenic Kras in hematopoietic cells initiates a rapidly fatal myeloproliferative disorder. *Proc Natl Acad Sci USA* 101(2):597–602.
21. Chan IT, et al. (2004) Conditional expression of oncogenic K-ras from its endogenous promoter induces a myeloproliferative disease. *J Clin Invest* 113(4):528–538.
22. Menzies AM, Long GV (2014) Dabrafenib and trametinib, alone and in combination for BRAF-mutant metastatic melanoma. *Clin Cancer Res* 20(8):2035–2043.
23. Schadendorf D, et al. (2014) Functional and symptom impact of trametinib versus chemotherapy in BRAF V600E advanced or metastatic melanoma: Quality-of-life analyses of the METRIC study. *Ann Oncol* 25(3):700–706.